

Comparative Evaluation of Laser Induced Graphene (LIG) Traces on Polyimide under Soft and Hard Stress for IoT Applications

Alessio Mostaccio, *Graduate Student Member, IEEE*, Gianni Antonelli, Mario Bragaglia Eugenio Martinelli, and Gaetano Marrocco, *Senior Member, IEEE*

Abstract—Laser-induced graphene (LIG) is an emerging manufacturing technique for engraving graphene patterns on precursor substrates. LIG has great potential applications to flexible eco-friendly and wrapping electronics devices such as on-skin sensors and antennas for human body physiological monitoring. Moreover, LIG-made electronic labels could be embedded into innovative food packages to reduce contamination and waste. As the so-obtained conducting graphene traces form a non-homogeneous and partly volatile structure, it strongly interacts with the external environment. This paper resumes a unitary experimental campaign to quantify the stability of the sheet resistance of LIG traces against several external stimuli, such as temperature and humidity gradients, contact with dry and wet objects, and cyclic bending. The results indicate that their effects depend on the tuning parameters of the laser and, in particular, on the power and beam defocusing. The sheet resistance variation during temperature and humidity stress is relatively modest and generally reversible by resorting to a 9 W beam with a few defocusing that generates a very compact and robust graphene substrate. The cyclic touch with dry and especially with wet objects can instead produce a more remarkable variation of the resistance and even permanent degradation of the surface depending on the specific lasing parameters.

A conservative $\pm 30\%$ uncertainty of the nominal sheet resistance hence must be included in the electromagnetic simulations of LIG-based devices to account for unpredictable dynamic interactions with real-life objects.

Index Terms—Graphene, Flexible Antenna, Sensors, LIG, Polyimide, IoT.

I. INTRODUCTION

SINCE its discovery, the outstanding properties of graphene have attracted the attention of the scientific community [1]. Unfortunately, its manufacturing complexity still hinders its large-scale deployment [2]. Thus, in the past decade, laser induction techniques have been proposed as novel methods to directly scribe graphene on polymeric substrates through an easy, fast, and low-cost process [3], [4]. For its ability to react to physical / chemical stimuli, laser-induced graphene (LIG) has been widely used for sensing purposes so far [5]. For the most part, the resulting sensors are a few millimeters in size and have been integrated into wired systems and interconnected to conventional acquisition boards. Examples concern sensors for strain/bending [6]–[9], pressure [10]–[12],

gas [13], [14], temperature and relative humidity (RH) [15]–[18]. Nevertheless, other common LIG applications refer to supercapacitors [19], [20], electrodes, and triboelectric nanogenerators [21].

More recently, LIG technology has also been tested to manufacture simple flexible antennas. In particular, [22] proposed a hybrid graphene-MoS polygonal monopole with coplanar feeding engraved on several substrates with performance comparable to its copper counterparts. A 5.8 GHz patch antenna made by LIG was analyzed in [23] to measure the strain of the human body by exploiting the natural change in the conductivity of graphene in reaction to surface deformation. [24] reports a LIG patch antenna on a cellulose substrate for eco-friendly applications. Furthermore, [25] employed this technique for the manufacturing of UHF RFID tags, and [26] exploited LIG for the fabrication of wearable monopoles in the S-band.

Therefore, despite the fact that the use of LIG technology for antennas is still in the initial phase, possible applications in IoT (Internet of Things), and in particular to smart-plaster for human body monitoring [27]–[29] and to smart packaging for low-cost food control [30] and recycling, could boost the large-scale diffusion of this technology.

Antennas have unique features compared to smaller LIG-based devices. In particular, they have large size (typically comparable with a wavelength) so that *i*) they will be bent with a small curvature radius when attached onto objects or the human skin [27], [31]; *ii*) they are generally exposed, in real applications, to unpredictable environmental conditions (variable temperature and humidity, at least); *iii*) they could undergo mechanical stress such as the touch with hard objects [32] producing pressure on the LIG surface and, not least, *iv*) they could come in touch with wet materials that release water moisture, such as the skin or food and vegetables [33]. All the above phenomena are expected to produce a temporary or permanent modification of the LIG's intimate structure. The proper design of LIG antennas must therefore adequately account for the possible variation or uncertainty in the sheet resistance of the LIG in real conditions.

The morphology as well as the intimate structure of LIG have been already demonstrated to be responsible for the variation of its properties to external stimuli and have been also exploited to achieve sensing functionalities for stress and pressure. As a matter of fact, the fluffy morphology of LIG makes it naturally sensitive to external compression

The authors are with the Pervasive Electromagnetics Lab, the Bioinspired Electronic Engineering group, University of Rome Tor Vergata, Via del Politecnico 1, Rome, Italy (e-mail: alessio.mostaccio@uniroma2.it, g.antonelli@ing.uniroma2.it, bragaglia@ing.uniroma2.it, martinelli@ing.uniroma2.it, gaetano.marrocco@uniroma2.it)

which causes the decrease of the interlayer distance and thus it increases the conductivity [34], [35]. In addition, another cause of modification of the LIG's conductivity can be the random contact with suspended nanofibers or the synchronous shearing of the latter when an ordered morphology prevails [36]. In the case of bending, instead, the leading phenomenon is the temporary disconnection of the fibres [9], [37], [38]. Furthermore, Luo et al. [39] discovered that the higher the power / scan speed ratio, the higher the sensitivity to the enforced stress since higher powers are related to a more porous structure which is easily disrupted when the load is applied. Above studies are however mostly oriented to sensing applications while less focused to durability. The tests were referred to not homogeneous kinds and sizes of LIG samples as well as the performance indicators were generally different.

This paper proposes a comprehensive and unitary evaluation campaign, referred to some meaningful manufacturing laser settings (power, speed, and the beam cross-section) that produce LIG samples of different morphology and electrical properties. LIG strips of the same sizes and derived from a polyimide (PI) substrate as precursor, were comparatively exposed, through simple protocols, to hard and soft stimuli that are expected to arise in future IoT applications of LIG devices in health, food, and pharma. We considered cyclic exposure to humidity gradients and surface stress by dry and wet touching and bendings. We can therefore quantify their impact on the same performance parameter, namely the sheet resistance that is the key LIG feature in the design of radiofrequency devices, antennas as first.

The paper is organized as follows. Section II introduces the considered manufacturing process of LIG, the materials and equipment, and the method for the electrical measurement of the sheet resistance. The measurement campaign is described in Section III concerning the application of stressful, soft (temperature and humidity) and hard (cyclic bending, dry and wet touch) stimuli. The obtained results, in terms of variation of the sheet resistance of the LIG samples, are then reported and discussed in Section IV and, finally, conclusions are drawn in Section V.

II. LIG MANUFACTURING AND CHARACTERIZATION

LIG is obtained through a photothermal process in which a CO_2 laser breaks the covalent bonds between the carbon and other atoms inside a polymer. Initially, the polymeric substrate, denoted as "precursor", is carbonized and produces amorphous tetrahedral carbon. As the CO_2 laser generates a beam with a wavelength of approximately $10 \mu m$, the process starts as soon as photons penetrate the substrate, even if their energy is not sufficient to directly break covalent bonds in which carbon is involved. However, they are powerful enough to make the chemical structure of PI vibrate, thus producing a huge local temperature increment ($> 2500 \text{ }^\circ C$) [4]. This leads to the breakage of the bonds among the atoms, moving from the existing sp^3 hybridization to sp^2 [40]. In this second phase, there is an increase in the electrical conductivity of the substrate and a rapid formation of gaseous products,

especially H_2 , CO_2 , and $C_xH_yN_z$ species. An aspiration system removes these waste products that are hazardous to human health. At the same time, the suction of graphene occurs, and LIG assumes the characteristic foam morphology [3].

A. Lasing

LIG samples considered next were fabricated starting from the precursor of PI sheets ($125 \mu m$ thick), from Dupont. The laser engraver was the Trotec Speedy 100 cutter. All the samples were manufactured in natural room conditions approximately corresponding to temperature $T = 25 \text{ }^\circ C$ and $RH = 60 \%$. The machine was set in pulsed and raster mode, with fixed pulses-per-inch $PPI=1000$. The laser engraving is hence carried along a dense alignment of parallel graphene lines, filling the surface. Three different LIG samples were obtained by proper combination of the main laser parameters, namely the laser power (P), the scan speed (V_s), and the beam defocusing. The first two have the most significant impact [41] on the morphology and electrical and mechanical properties [42] of the LIG, namely determining the depth of the trace and the amount of graphene produced. Laser defocusing is a second-order parameter to fine-tune the process [43] and is achieved by adding an offset h to the vertical axis of the laser head. Therefore, the beam footprint in the dielectric layer will widen, producing a partial overlap between adjacent lased spots [44] with an expected improvement in graphene homogeneity and conductivity.

B. LIG Samples

Starting from a preliminary literature scouting [41], [44]–[46], we identified some sets of the lasing parameters that are expected to provide a variety of LIG samples concerning the morphology (compact, fluffy) and electrical properties (high and low sheet resistance). The three settings, hereafter denoted as LIG-1, LIG-2, LIG-3, are reported in Table I. The first two differ for the scan speed V_s and for the laser power P . LIG-3 is similar to LIG-2 apart for a beam defocusing by the offset $h = 3 \text{ mm}$ which is expected to produce a more homogeneous scanning pattern. The samples have the shape of 5 cm by 1 cm strips. Magnified pictures of the strips' surface are reported in Fig. 1 as obtained in the macroscale by Analog Reflection Microscopy (AM - $0.7\text{-}4.5\times$ AmScope CL-SM-4TP), and then in the microscale by Field Emission Scanning Electron Microscope (FESEM, Zeiss Leo Supra 35, with settings: Electron High Tension EHT= 5 kV and Working Distance $WD=7 \text{ mm}$). The linear lasing pattern is clearly visible through the analog microscope in LIG-1 and LIG-3 samples. Instead, by increasing the laser power, more PI is converted into LIG, namely, the laser beam penetrates into a deeper thickness of the substrate. Accordingly, a disordered and hairy morphology prevails in the LIG-2 sample. The employment of laser defocusing in LIG-3 causes a further change in the sample morphology: the grey color of the LIG trace is lighter, making its appearance more similar to graphite rather than graphene. Furthermore, the overlap between two adjacent spots makes the engraving lines more blurry than

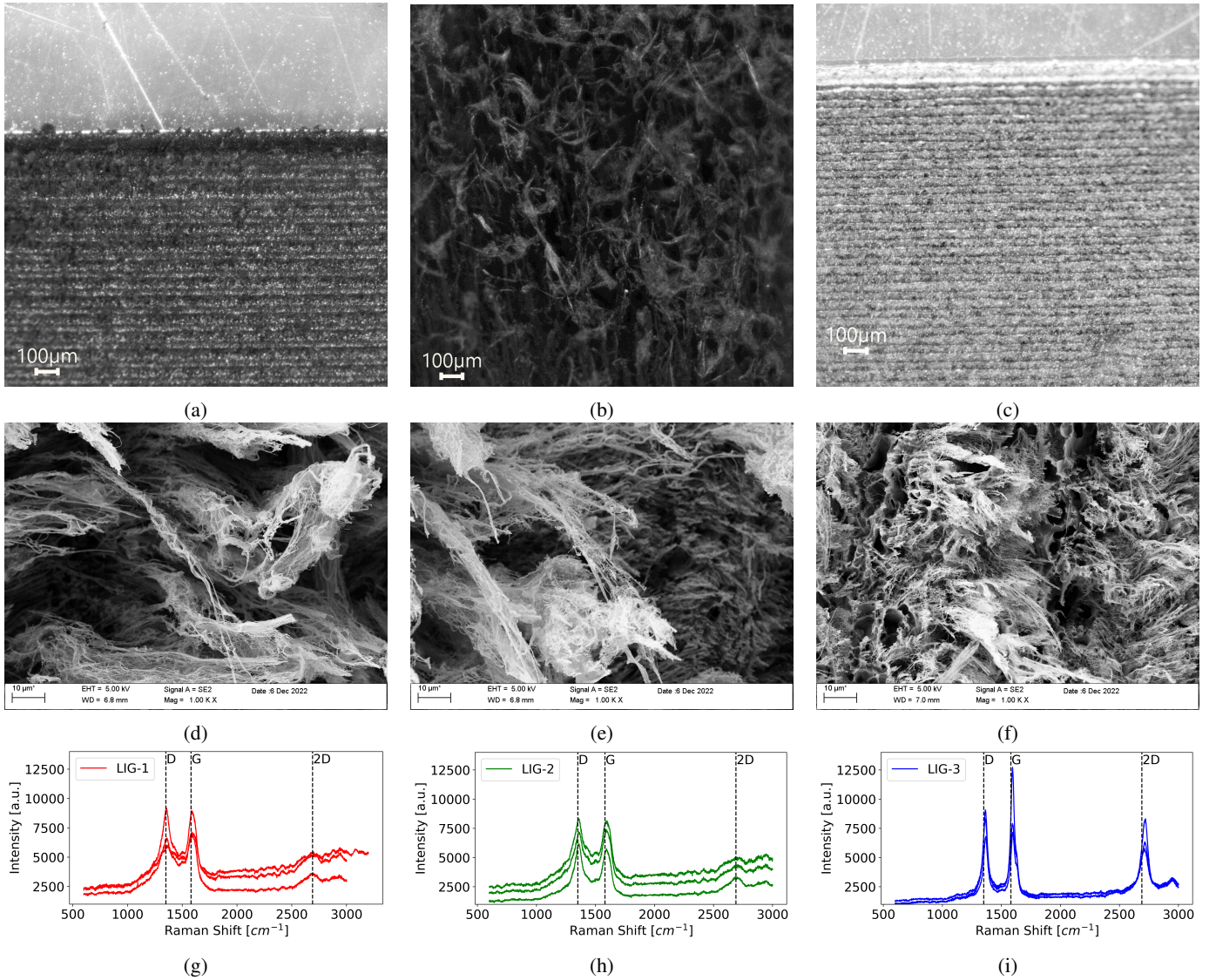


Fig. 1: (a)-(c) AM images of the three different LIG morphologies achieved with laser settings in Table I. The scale bar is set to 100 μm . (d)-(f) SEM magnification of the three LIG morphologies. The scale bar is set to 10 μm . (g)-(i) Intensity of the Raman shift measured at three points for each LIG sample. The vertical lines indicate the D, G, and 2D peaks respectively.

TABLE I: Summary of the laser settings employed for each LIG sample

Configuration	Power [W]	Scan speed [cm/s]	Offset [mm]	R_s [Ω/\square]	I_D/I_G	I_{2D}/I_G
LIG-1	3.5	4.2	0	43.7 ± 0.3	0.94 ± 0.07	0.63 ± 0.10
LIG-2	9	10	0	33.4 ± 0.3	1.04 ± 0.06	0.62 ± 0.01
LIG-3	9	10	3	12.3 ± 0.3	0.99 ± 0.13	0.84 ± 0.11

in LIG-1 [44]. The overall appearance is thus more compact. The microscale SEM scan reveals a fibrous morphology in all cases. Nevertheless, LIG-1 and LIG-2 are more porous than LIG-3 whose appearance is instead denser by the effect of beam defocusing. Further physical insight comes from the Raman spectroscopy performed at three points of each sample (Fig.1g-1i). The analysis of the spectra, and in particular of the graphene's characteristic peaks D, G and 2D, shows a similarity of the profiles of LIG-1 and LIG-2 (defective for the most) which differ from that of LIG-3. The ratio I_D/I_G

among the first two peaks (related to the sp^2 -hybridized carbon network and to the presence of defects within the structure, respectively) is close to 1 for all the LIGs (Table I) thus confirming the crystallinity of the ablated surface [41], [47]. In the case of LIG-3, instead, I_{2D}/I_G increases, and this is an indication of the decrease of the number of graphene layers [41], [47].

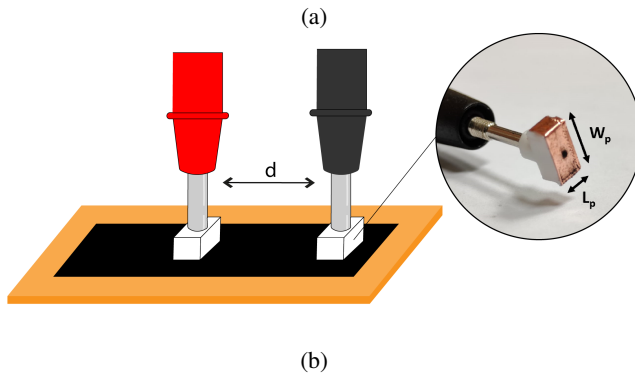
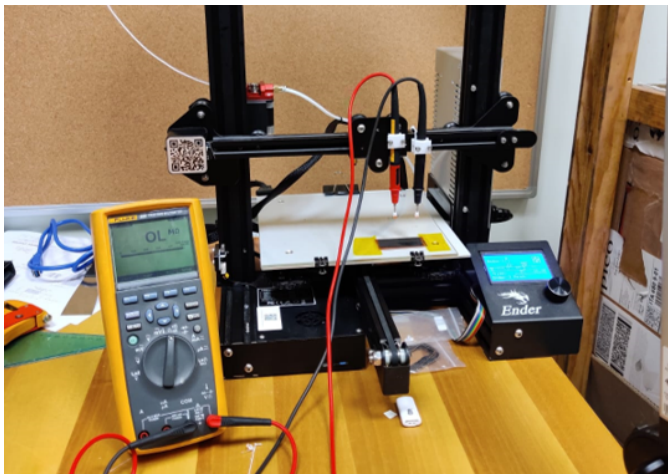


Fig. 2: (a) Measurement setup to evaluate the sheet resistance. Each probe is attached to the 3-axes positioner to precisely control the distance. (b) Schematic representation and prototype of the TLM probes

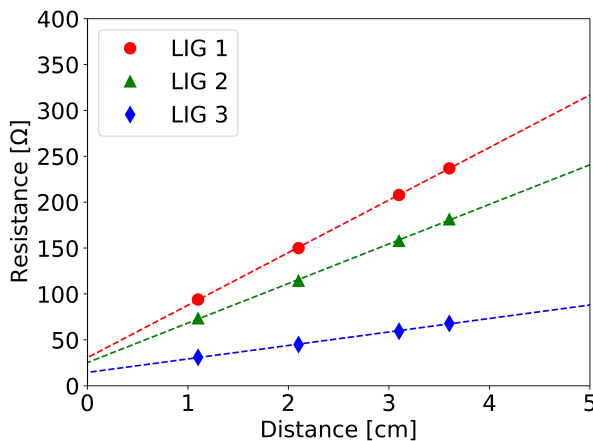


Fig. 3: Measured resistance between the probes in Fig. 2b versus the distance. The dashed lines are the LSQ regression.

C. Electrical characterization of the Sheet Resistance

The reference metric for the performance of LIG traces as conductors is the sheet resistance (R_s) that represents the resistance of a square sample of the conductor. The parameter is hence evaluated by means of the Transfer Length Method (TLM) [48]. It permits to drop out the edge effect and, in particular, the contact resistance at the interface with

metallic conductors (here the measurement probes) that is not negligible for semiconductors, and above all for graphene [49].

TLM is applied through a two-points measurement of resistance at increasing inter-distance d along the strip (Fig. 2b). For this purpose, we used the multimeter Fluke 289. For each configuration, four values of resistance were achieved as the result of an averaging process on three different samples and by varying the distance d . Measured resistance w.r.t. to the distance concentrates along the line (1)

$$R = \frac{R_s}{W_p} d + 2R_c \quad (1)$$

where R_c is the contact resistance. The sheet resistance is then estimated by extracting the slope of the measurements' distribution through Least Squares method and the mean square error (MSE) is reported as an indication of uncertainty.

The probes of the multimeter are made of rectangular conductive pads, with size $L_p = 0.75$ cm and $W_p = 0.4$ cm (Fig. 2b), wrapped onto 3D-printed holders. To ensure the repeatability, and to fix the probes on the LIG samples, a numerically controlled 3-axis positioner with 0.1 mm precision (Fig. 2a) is used to precisely translate the probes along the strip thus avoiding conductive epoxy glue that would inevitably induce artifacts in the measurement of the sheet resistance.

Raw measured data are reported in Fig. 3 and the estimated sheet resistance in Table I. A lower sheet resistance is related to high laser power [41] since the higher the power, the more PI is converted into LIG. We experimentally verified that a further power increment causes the destruction of the PI sample. As expected, beam defocusing produces a further reduction of the sheet resistance since the improved quality of graphene and homogeneity of the sample grant better conductivity [44]. It is worth noting that the standard deviation among measurements on the three samples for each kind of LIG are very small (roughly $0.3 \Omega/\square$) so the manufacturing can be considered rather reproducible.

III. DESIGN OF EXPERIMENTS

Two sets of stressful agents are here considered, referred as *soft stimuli* produced by the environment, such as gradients of external temperature and humidity, and then *hard stimuli* that are hence directly enforced onto the LIG samples, namely cycles of bending and of contact with dry and wet objects. Each test is applied to three novel LIG samples for each group of lasing settings to also evaluate the repeatability of the achieved performances. The second set of tests accounts for possible interactions of LIG antennas with the human body that deforms thousand times per day and that can interact with hands, textiles, and contacting objects. The interaction with wet objects could moreover be related to the application to fresh food monitoring. The test methodologies are described here, while the results of measurements are resumed in the next Section. The purpose is to quantify the variation of the sheet resistance during and after the tests as well as to analyze the eventual permanent degradation of the surface.

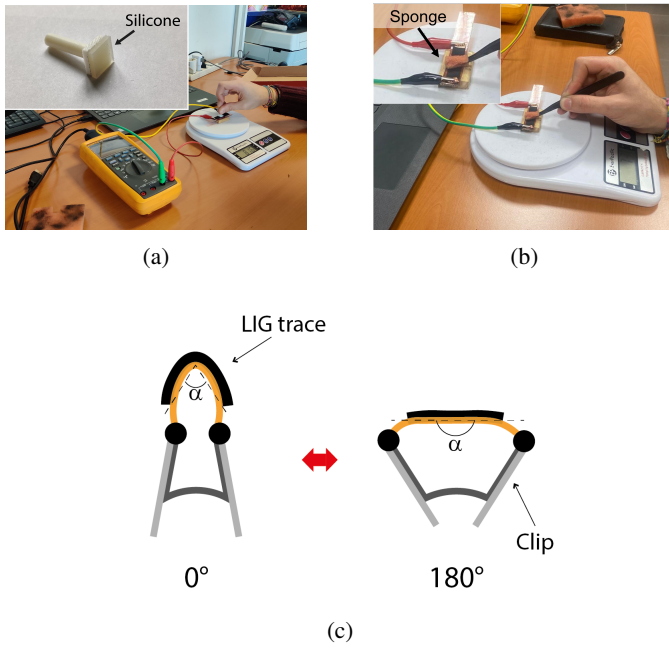


Fig. 4: (a) Photo of the cyclic contacts with a dry object. The silicone probe (inset) is manually put in touch with the LIG sample and the LIG resistance is measured by the multimeter. A same force touch is enforced in each cycle with the help of a digital scale. (b) The same setup was employed for the cyclic contact with a wet object wherein a sponge was employed. (c) Arrangement of the paper clip for the bending test.

A. Soft Stimuli

The following experiments involve the climatic chamber (Binder Mk-56) to enforce gradients of temperatures and humidity. The multimeter's probes are hence inserted inside the chamber and the sheet resistance is measured continuously during the test. The following two cycles are applied.

1) *Temperature cycle*: The temperature is linearly raised between 15°C and 85°C and return, with a fixed relative humidity $\text{RH} = 30\%$.

2) *RH cycle*: The temperature is kept fixed to 40°C and the relative humidity is monotonically increased (through a step-wise dynamics) from 20% to 80% and return.

The overall impact of the exposure to external humidity is the combination of some competing phenomena. *i*) The water molecules can lead to ionic conduction upon the surface of LIG thus decreasing the measured sheet resistance [50], [51]. *ii*) Simultaneously, for prolonged exposure to high external humidity, water molecules can infiltrate in between the flakes, determining the opposite effect [52]. Due to the swelling phenomenon, indeed, these molecules increase the inter-layer distance, augmenting the semiconductor discontinuity as well [51]. *iii*) Finally, the presence of defects in the substrate [53], its hydrophobicity, as well as the amount of oxygenated functional groups inside the graphene [51], are expected to improve the overall conductivity, thus decreasing the sheet resistance.

The sensitivity of the LIG samples to the above stimuli is evaluated by considering the median value of the measured

resistance in the last 5 min of each step of the ascending profile. Then, the values of R_s w.r.t. temperature and RH were interpolated with a linear and quadratic fitting, respectively, which minimise the MSE. The slope of the line, as well as the coefficient of the quadratic term, and their relative error, were reported as indications of the sensitivity $S_{T/RH}$.

B. Hard Stimuli

1) *Cyclic contacts with a dry object*: The LIG sample is cyclically touched by a silicone probe (a silicone rubber slab attached onto a plastic stick - inset Fig. 4a) for 5 s and then the probe is released and applied again for overall twelve touches in 2 min while the sheet resistance is continuously recorded. A similar applied pressure is enforced in each cycle by the help of a digital scale.

Also in this case, there are competing phenomena occurring during contacts: on one side the contact leads to the removal of LIG flakes from the surface of the precursor substrate thus determining an increment of the sheet resistance; on the other side, instead, the applied pressure produces a compression of the surface morphology so that the distance between adjacent flakes is narrowed thus reducing the sheet resistance [36], [52]. The impact of this mechanical stress is evaluated both in terms of resistance variation and of surface degradation by an *adhesion test* [45], namely by visualizing the residual graphene particles on the touching probe at the end of the experiment. The photos will hence provide further physical insight on the compactness of the fabricated graphene surface.

2) *Cyclic contacts with a wet object*: The contact with liquids is emulated by bringing the LIG sample in touch with a wet sponge with negligible pressure (Fig. 4b). Accordingly, water molecules concentrate on the sample surface and gently infiltrate in between the LIG flakes.

3) *Cyclic bending*: The bending or the stretching of the LIG trace determines the disconnection of the inner flakes, as well as internal cracks that may lead to a conductivity decrement and thus to an increment of the resistance [9]. Each LIG sample is attached to a paper binding clip (scheme in Fig. 4c) which permits to bend the strip up to 180° . In the specific, when the clip is open ($\alpha = 180$, ideally), the LIG strip is unaltered, while when the clip is closed ($\alpha = 0$), the strip is bent at nearly 180° . The clip is cyclically opened and closed twelve times for 2 min (5 s periodicity).

We considered two performance metrics in each test:

- the average peak variation of the sheet resistance (ΔR_S^p) when the stimulus is applied

$$\Delta R_S^p = \frac{1}{N \cdot M} \sum_{i=1}^M \sum_{k=1}^N \frac{R_{s,i}(k) - R_{s,i0}(k)}{R_{s,i0}(0)} \quad (2)$$

where $N = 12$ is the total number of stimuli during the experiment, $M = 3$ is the number of samples for each LIG configuration, $R_{s,i}(k)$ the median value of sheet resistance of i -th sample during the k -th stimulus, $R_{s,i0}(k)$ the median value of resistance before the k -th stimulus, and $R_{s,i0}(0)$ the resistance of the unperturbed i -th sample.

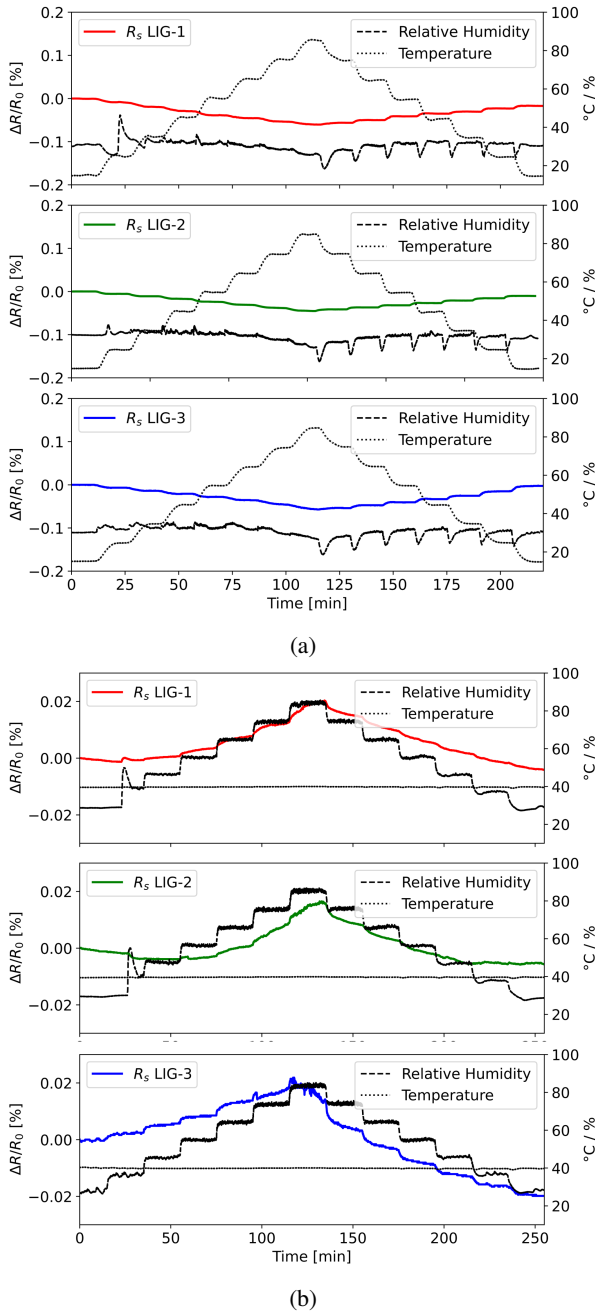


Fig. 5: (a) Example of variation of sheet resistance due to Temperature and (b) of RH gradients for a sample of each type of LIG.

- the variation of sheet resistance after each stimulus w.r.t. the initial value (ΔR_S^T) averaged on all cycles. The latter is computed as the slope of the line which best fits the distribution

$$\Delta R_S^T = \text{slope} \left(k, \frac{R_{s,i0}(k) - R_{s,i0}(0)}{R_{s,i0}(0)} \right)_{i=1 \dots M} \quad (3)$$

$$k = 1 \dots N$$

IV. RESULTS OF TESTS

The numerical results of the tests described in the previous Section are reported next.

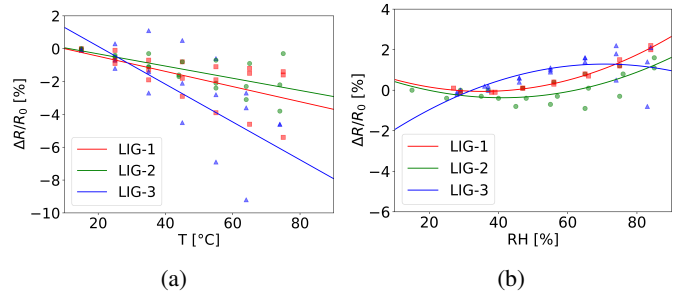


Fig. 6: Cumulative relationship between sheet resistance and Temperature (a) and RH (b) for each LIG configuration. Continuous lines are linear and quadratic fitting respectively.

TABLE II: Sensitivity to variable environmental conditions with respect to LIG configuration

Configuration	$S_T [\Delta R\% C^{-1}]$	$S_{RH} [\Delta R\% \Delta RH\%^{-1}]$
LIG-1	-0.05 ± 1.21	$(0.9 \pm 7) \cdot 10^{-3}$
LIG-2	-0.04 ± 0.56	$(0.8 \pm 197) \cdot 10^{-3}$
LIG-3	-0.11 ± 4.71	$(-0.9 \pm 302) \cdot 10^{-3}$

A. Results of Soft Stimuli tests

Diagrams in Fig. 5 show an example of the measured variation of the sheet resistance for the three LIG configurations produced by the temperature and by the humidity transients.

Overall, the impact of temperature and humidity gradients on the sheet resistance is rather modest, with peak variations below 0.1%. Anyway, due to the lack of oxygenated groups, which increase the conductivity [51], temperature and RH have opposite impacts. Sheet resistance indeed reduces along with temperature rise, which is typical of semiconductors [15], while the humidity produces an increase of the resistance. Accordingly, the effect of water absorption generally dominates on the ionic conduction and on the absence of oxygenated functional groups either in the substrate or in the LIG trace [52]. The resulting sensitivities of the sheet resistance to temperature and humidity changes, as evaluated from the ascending gradients of Fig. 6, are reported in Table II. LIG-1 and LIG-2 perform almost equally with a sensitivity of the sheet resistance to the temperature of about $-0.04 \% C^{-1}$ in agreement with other results [54]. LIG-3, instead, exhibits a more sensitive behaviour. This phenomenon is explained and corroborated by the Raman spectra of the three samples (Fig. 1g-1i) which highlighted a similarity of the intimate structure of LIG-1 and LIG-2 which instead differs from that of LIG-3.

A similar trend is also exhibited when RH cycles are enforced. As a matter of fact, by observing the sign of the sensitivity in the case of LIG-1 and LIG-2, the higher the RH the more water molecules are absorbed and thus the higher the sheet resistance is. When considering LIG-3, the resistance increases along with the RH up to 60%; above this value, instead, water molecules are not absorbed anymore but they deposit upon the surface of LIG decreasing the sheet resistance [50].

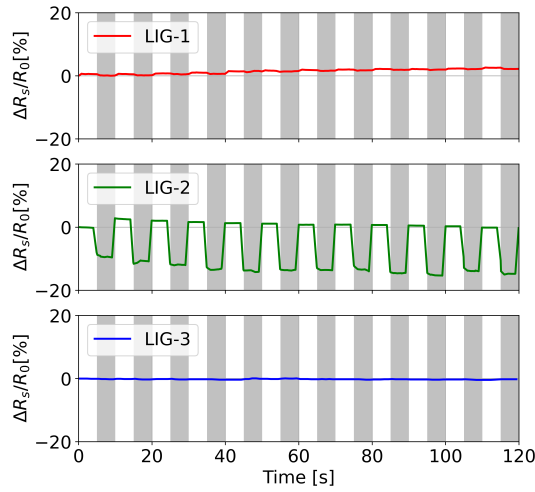


Fig. 7: Dry touch test. Example of variation of the sheet resistance of the three LIG samples during cyclic contacts (gray bands) by a silicone probe.

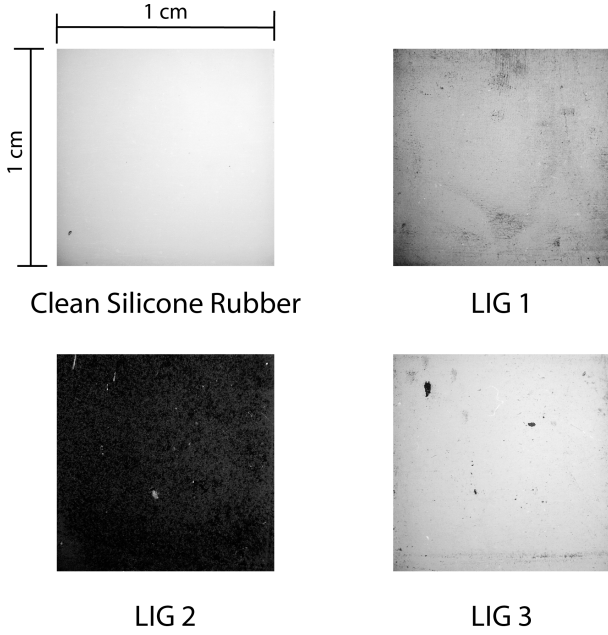


Fig. 8: Adhesion test. Residual graphene particles on the silicone touching probe after the 12 cyclic touches.

B. Results of Hard Stimuli tests

1) *Dry contacts*: Fig. 7 shows an example of the measured variation of the sheet resistance of the three LIG configurations during the cyclic touch of the silicone probe. The residual graphene on the probe is instead reported in Fig. 8. The effect of the dry touching is strictly dependent on the morphology of the graphene and it is summarized in Table III. LIG-2 has a higher value of ΔR_S^p (about -12.7% of its initial value) than LIG-1 and LIG-3. Due to the fluffier morphology, indeed, the applied pressure causes the temporary connection of the superficial suspended nanofibers [36] which instead are lower in the case of LIG-1 or even absent (LIG-3). Accordingly,

TABLE III: Averaged peak and total variation of sheet resistance in case of periodic contacts with a silicone probe

Configuration	ΔR_S^p [Ω/\square]	ΔR_S^T [Ω/\square]
LIG-1	-0.26 ± 0.32	0.04 ± 0.03
LIG-2	-12.7 ± 2.97	0.00 ± 0.12
LIG-3	-0.25 ± 0.52	0.00 ± 0.06

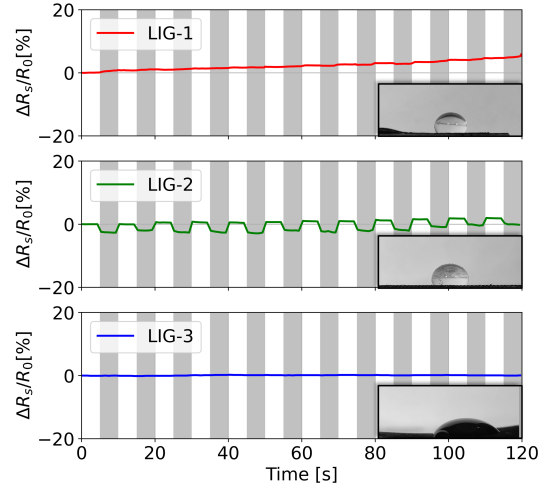


Fig. 9: Wet touch test. Example of variation of the sheet resistance when the three LIG samples are cyclically put in touch with a wet sponge. Water droplet displacement over the surface of each LIG type in the insets.

TABLE IV: Averaged peak and total variation of sheet resistance in case of periodic contacts of LIGs with a wet sponge.

Configuration	ΔR_S^p [Ω/\square]	ΔR_S^T [Ω/\square]
LIG-1	0.28 ± 0.37	0.40 ± 0.07
LIG-2	-4.34 ± 3.11	0.23 ± 0.17
LIG-3	-0.19 ± 0.25	-0.07 ± 0.12

the number of particles collected by the silicone probe is significantly higher in the case of LIG-2. By comparing the value of ΔR_S^T , LIG-1 exhibits a progressive increase of the sheet resistance while LIG-2 is more durable over the time. This is explained by the lower engraving power which accordingly reduces the amount of LIG produced. Finally, no flakes are released by LIG-3 which indeed is characterized by a dense aspect (Fig. 1f). Therefore, the variations of conductivity, both instantaneous and permanent, due to the stimulus are insignificant.

In conclusion, we can assert that for LIG-1 and LIG-3, the compression of the inner flakes/layers dominates in agreement with [36].

2) *Wet contacts*: With reference to Fig. 9, the touch interaction with a humid object is impacting on the performance of both LIG-1 and LIG-2 (Table IV). Similarly to the previous experiments, the results vary according to the morphology.

In agreement with the previous test, the applied pressure, despite being lower in this case, causes a decrement of sheet resistance. The infiltration of water molecules within the flakes

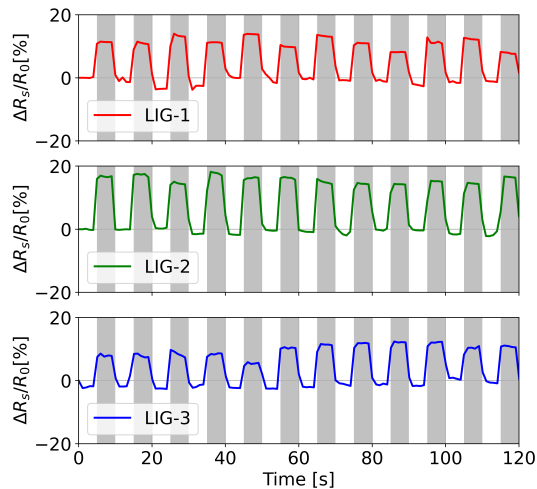


Fig. 10: Bending Test. Example of variation of the resistance for each LIG configuration due to the repeated bending of the sample. The grey and white zones correspond to the bending and non-bending periods, respectively.

TABLE V: Averaged peak and total variation of sheet resistance in case of periodic bending.

Configuration	ΔR_S^P [Ω/\square]	ΔR_S^T [Ω/\square]
LIG-1	12.6 ± 2.75	-0.12 ± 0.11
LIG-2	22.9 ± 8.95	0.06 ± 0.17
LIG-3	14.8 ± 6.89	0.03 ± 0.08

slightly degrades the samples. LIG-1 and LIG-2 are indeed characterized by a progressive increment of sheet resistance of roughly 0.40% and 0.23% per touch, respectively. Instead, the compactness of LIG-3 hinders the infiltration and, on the contrary, fosters the accumulation of water molecules upon the surface. As a result, the sheet resistance is generally reduced thanks to the ionic conduction mechanism [50].

3) *Bending test*: The results of the cyclic bending test are reported in Fig. 10 and resumed in Table V. All the samples of LIG show a remarkable increment of sheet resistance (from 10% to 30% of their initial value) when bent. As in the previous tests, LIG-2 is more sensitive since the hairy morphology is more prone to flake disconnection. Nevertheless, none of the LIG types exhibit a significant degradation over time.

V. SUMMARY AND CONCLUSION

The main findings of the experimental tests reported in the paper are resumed next and vary according to the kind of stimulus.

- The atomic structure of graphene affects the sensitivity of the sheet resistance to soft stimuli while differences in the morphology dominate when hard stresses, namely contacts with dry and wet objects, and the bending, are applied.
- Temperature and humidity gradients have a negligible impact on the sheet resistance of LIG samples independently on the lasing settings, in agreement to [52], [54].

- Interactions with a dry object have a small impact in the case of dense LIG (less than 1% variation of its initial sheet resistance). Instead, fluffier morphologies (LIG-2) produce a higher variation of the sheet resistance up to 10% the unperturbed value in agreement with [9], [12], [36].
- The interaction with wet objects generally produces a *permanent* and *incremental* rise of the resistance.
- The above detrimental effects are greatly minimized by resorting to a lasing process exploiting a broad beam cross-section that makes the graphene layer more compact.
- Bending is definitely the most impacting stressful agent among those considered, with variations of sheet resistance above 20% of the unperturbed value. This effect could potentially degrade the performance of LIG-made stretchable antennas for application on human skin.

Overall, the experimental tests confirmed that the achievable electrical features are reproducible and well-controllable by the lasing settings, and therefore we expect that reliable numerical electromagnetic simulations in unperturbed conditions can be fed by knowing LIG parameters. The LIG technology allows a selective manufacturing of complex IoT wireless devices so that the communication and sensing sub-modules can be fabricated by the most appropriate graphene morphology. Laser settings corresponding to LIG-3, which guarantee the lowest sheet resistance, should be exploited for the radiating region to achieve the best communication performance. The sensitive part of the device, instead, (for instance interdigital capacitors) could benefit of lasing settings as for LIG-2 that amplify the sensitivity to external stimuli. In any case, the profile of sheet resistance in response to hard external agents is characterized by a not negligible standard deviation due to the disordered displacement of nanoflakes. Accordingly, the numerical simulation of a radiofrequency device, especially at the IoT frequencies (some gigahertz), must conservatively include a $\pm 30\%$ uncertainty around the nominal sheet resistance to estimate the achievable communication performance in real unpredictable conditions.

ACKNOWLEDGMENTS

The authors wish to thank prof. Silvia Orlanducci for valuable technical and scientific support for Raman scattering analysis.

The work was partially supported by Rome Technopole in the framework of the National Recovery and Resilience Plan (NRRP), NextGenerationEU.

REFERENCES

- [1] J. Phiri, P. Gane, and T. C. Maloney, "General overview of graphene: Production, properties and application in polymer composites," *Materials Science and Engineering: B*, vol. 215, pp. 9–28, 2017.
- [2] C. Soldano, A. Mahmood, and E. Dujardin, "Production, properties and potential of graphene," *Carbon*, vol. 48, no. 8, pp. 2127–2150, 2010.
- [3] J. Lin, Z. Peng, Y. Liu, F. Ruiz-Zepeda, R. Ye, E. L. Samuel, M. J. Yacaman, B. I. Yakobson, and J. M. Tour, "Laser-induced porous graphene films from commercial polymers," *Nature communications*, vol. 5, no. 1, pp. 1–8, 2014.

- [4] L. Wang, Z. Wang, A. N. Bakhtiyari, and H. Zheng, "A comparative study of laser-induced graphene by co₂ infrared laser and 355 nm ultraviolet (uv) laser," *Micromachines*, vol. 11, no. 12, p. 1094, 2020.
- [5] L. Huang, J. Su, Y. Song, and R. Ye, "Laser-induced graphene: En route to smart sensing," *Nano-micro letters*, vol. 12, no. 1, pp. 1–17, 2020.
- [6] A. F. Carvalho, A. J. Fernandes, C. Leitão, J. Deuermeier, A. C. Marques, R. Martins, E. Fortunato, and F. M. Costa, "Laser-induced graphene strain sensors produced by ultraviolet irradiation of polyimide," *Advanced Functional Materials*, vol. 28, no. 52, p. 1805271, 2018.
- [7] S.-Y. Jeong, Y.-W. Ma, J.-U. Lee, G.-J. Je, and B.-s. Shin, "Flexible and highly sensitive strain sensor based on laser-induced graphene pattern fabricated by 355 nm pulsed laser," *Sensors*, vol. 19, no. 22, p. 4867, 2019.
- [8] L. Huang, H. Wang, P. Wu, W. Huang, W. Gao, F. Fang, N. Cai, R. Chen, and Z. Zhu, "Wearable flexible strain sensor based on three-dimensional wavy laser-induced graphene and silicone rubber," *Sensors*, vol. 20, no. 15, p. 4266, 2020.
- [9] B. Kulyk, B. F. Silva, A. F. Carvalho, S. Silvestre, A. J. Fernandes, R. Martins, E. Fortunato, and F. M. Costa, "Laser-induced graphene from paper for mechanical sensing," *ACS Applied Materials & Interfaces*, vol. 13, no. 8, pp. 10210–10221, 2021.
- [10] D. Wu, Q. Peng, S. Wu, G. Wang, L. Deng, H. Tai, L. Wang, Y. Yang, L. Dong, Y. Zhao, *et al.*, "A simple graphene nh₃ gas sensor via laser direct writing," *Sensors*, vol. 18, no. 12, p. 4405, 2018.
- [11] S.-Y. Xia, Y. Long, Z. Huang, Y. Zi, L.-Q. Tao, C.-H. Li, H. Sun, and J. Li, "Laser-induced graphene (lig)-based pressure sensor and triboelectric nanogenerator towards high-performance self-powered measurement-control combined system," *Nano Energy*, vol. 96, p. 107099, 2022.
- [12] A. Kaidarova, N. Alsharif, B. N. M. Oliveira, M. Marengo, N. R. Galdi, C. M. Duarte, and J. Kosel, "Laser-printed, flexible graphene pressure sensors," *Global Challenges*, vol. 4, no. 4, p. 2000001, 2020.
- [13] M. G. Stanford, K. Yang, Y. Chyan, C. Kittrell, and J. M. Tour, "Laser-induced graphene for flexible and embeddable gas sensors," *ACS nano*, vol. 13, no. 3, pp. 3474–3482, 2019.
- [14] F. Wang, K. Wang, B. Zheng, X. Dong, X. Mei, J. Lv, W. Duan, and W. Wang, "Laser-induced graphene: preparation, functionalization and applications," *Materials technology*, vol. 33, no. 5, pp. 340–356, 2018.
- [15] M. Marengo, G. Marinaro, and J. Kosel, "Flexible temperature and flow sensor from laser-induced graphene," in *2017 IEEE SENSORS*. IEEE, 2017, pp. 1–3.
- [16] S. Gandla, M. Naqi, M. Lee, J. J. Lee, Y. Won, P. Pujar, J. Kim, S. Lee, and S. Kim, "Highly linear and stable flexible temperature sensors based on laser-induced carbonization of polyimide substrates for personal mobile monitoring," *Advanced Materials Technologies*, vol. 5, no. 7, p. 2000014, 2020.
- [17] S. Yin, H. Ibrahim, P. S. Schnable, M. J. Castellano, and L. Dong, "A field-deployable, wearable leaf sensor for continuous monitoring of vapor-pressure deficit," *Advanced Materials Technologies*, vol. 6, no. 6, p. 2001246, 2021.
- [18] K. K. Adhikari, C. Wang, T. Qiang, and Q. Wu, "Polyimide-derived laser-induced porous graphene-incorporated microwave resonator for high-performance humidity sensing," *Applied Physics Express*, vol. 12, no. 10, p. 106501, 2019.
- [19] X. Shi, F. Zhou, J. Peng, R. Wu, Z.-S. Wu, and X. Bao, "One-step scalable fabrication of graphene-integrated micro-supercapacitors with remarkable flexibility and exceptional performance uniformity," *Advanced Functional Materials*, vol. 29, no. 50, p. 1902860, 2019.
- [20] A. Lamberti, F. Clerici, M. Fontana, and L. Scaltrito, "A highly stretchable supercapacitor using laser-induced graphene electrodes onto elastomeric substrate," *Advanced Energy Materials*, vol. 6, no. 10, p. 1600050, 2016.
- [21] M. G. Stanford, J. T. Li, Y. Chyan, Z. Wang, W. Wang, and J. M. Tour, "Laser-induced graphene triboelectric nanogenerators," *ACS nano*, vol. 13, no. 6, pp. 7166–7174, 2019.
- [22] M. R. Abdul-Aziz, S. A. Mohassieb, N. A. Eltresy, M. M. Yousef, B. Anis, S. O. Abdellatif, and A. S. Khalil, "Enhancing the performance of polygon monopole antenna using graphene/tmdcs heterostructures," *IEEE Transactions on Nanotechnology*, vol. 19, pp. 269–273, 2020.
- [23] B. Sindhu, A. Kothuru, P. Sahatiya, S. Goel, and S. Nandi, "Laser-induced graphene printed wearable flexible antenna-based strain sensor for wireless human motion monitoring," *IEEE Transactions on Electron Devices*, vol. 68, no. 7, pp. 3189–3194, 2021.
- [24] M. Ahmad, G. Cantarella, M. A. C. Angeli, M. Madagalam, C. Ebner, M. Ciocca, R. Riaz, P. Ibba, M. Petrelli, I. Merino, *et al.*, "2.4 ghz microstrip patch antenna fabricated by means of laser induced graphitization of a cellulose-based paper substrate," in *2021 IEEE International Flexible Electronics Technology Conference (IFETC)*. IEEE, 2021, pp. 0044–0046.
- [25] F. Chietera, R. Colella, A. Verma, E. Ferraris, C. E. Corcione, C. Moraila-Martinez, D. Gerardo, Y. Acid, A. Rivadeneyra, and L. Catarinucci, "Laser-induced graphene, fused filament fabrication, and aerosol jet printing for realizing conductive elements of uhf rfid antennas," *IEEE Journal of Radio Frequency Identification*, 2022.
- [26] A. Mostaccio, G. Antonelli, C. Occhiuzzi, E. Martinelli, and G. Marrocco, "Experimental characterization of laser induced graphene (lig) antennas for s-band wearable applications in 5g," in *2022 IEEE 12th International Conference on RFID Technology and Applications (RFID-TA)*. IEEE, 2022, pp. 51–54.
- [27] F. Naccarata, G. M. Bianco, and G. Marrocco, "Sensing performance of multi-channel rfid-based finger augmentation devices for tactile internet," *IEEE Journal of Radio Frequency Identification*, 2022.
- [28] C. Miozzi, G. Saggio, E. Gruppioni, and G. Marrocco, "Near-field circular array for the transcutaneous telemetry of uhf rfid-based implantable medical devices," *IEEE Journal of Electromagnetics, RF and Microwaves in Medicine and Biology*, 2021.
- [29] M. Caccami, M. Mulla, C. Di Natale, and G. Marrocco, "Wireless monitoring of breath by means of a graphene oxide-based radiofrequency identification wearable sensor," in *2017 11th European Conference on Antennas and Propagation (EUCAP)*. IEEE, 2017, pp. 3394–3396.
- [30] C. Occhiuzzi, F. Camera, M. D'Orazio, N. D'Uva, S. Amendola, G. M. Bianco, C. Miozzi, L. Garavaglia, E. Martinelli, and G. Marrocco, "Automatic monitoring of fruit ripening rooms by uhf rfid sensor network and machine learning," *IEEE Journal of Radio Frequency Identification*, 2022.
- [31] F. Camera, C. Miozzi, F. Amato, C. Occhiuzzi, and G. Marrocco, "Experimental assessment of wireless monitoring of axilla temperature by means of epidermal battery-less rfid sensors," *IEEE Sensors Letters*, vol. 4, no. 11, pp. 1–4, 2020.
- [32] M. Frattaioli, G. M. Bianco, S. Nappi, and G. Marrocco, "A finger-worn epidermal antenna for pressure sensing," in *2022 16th European Conference on Antennas and Propagation (EuCAP)*. IEEE, 2022, pp. 1–4.
- [33] G. M. Bianco and G. Marrocco, "Sensorized facemask with moisture-sensitive rfid antenna," *IEEE Sensors Letters*, vol. 5, no. 3, pp. 1–4, 2021.
- [34] A. Al-Hamry, Z. Xian, A. Adiraju, R. Ramalingame, D. Rejerandan, and O. Kanoun, "Performance of pressure sensors based on laser induced graphene material on polymeric coated substrate," in *2019 5th International Conference on Nanotechnology for Instrumentation and Measurement (NanofIM)*. IEEE, 2019, pp. 1–7.
- [35] H. Tian, Y. Shu, X.-F. Wang, M. A. Mohammad, Z. Bie, Q.-Y. Xie, C. Li, W.-T. Mi, Y. Yang, and T.-L. Ren, "A graphene-based resistive pressure sensor with record-high sensitivity in a wide pressure range," *Scientific reports*, vol. 5, no. 1, p. 8603, 2015.
- [36] L. Huang, Y. Liu, G. Li, Y. Song, J. Su, L. Cheng, W. Guo, G. Zhao, H. Shen, Z. Yan, *et al.*, "Ultrasensitive, fast-responsive, directional airflow sensing by bioinspired suspended graphene fibers," *Nano Letters*, 2023.
- [37] A. Kaidarova and J. Kosel, "Physical sensors based on laser-induced graphene: A review," *IEEE Sensors Journal*, vol. 21, no. 11, pp. 12426–12443, 2020.
- [38] A. Chhetry, M. Sharifuzzaman, H. Yoon, S. Sharma, X. Xuan, and J. Y. Park, "Mos₂-decorated laser-induced graphene for a highly sensitive, hysteresis-free, and reliable piezoresistive strain sensor," *ACS applied materials & interfaces*, vol. 11, no. 25, pp. 22531–22542, 2019.
- [39] S. Luo, P. T. Hoang, and T. Liu, "Direct laser writing for creating porous graphitic structures and their use for flexible and highly sensitive sensor and sensor arrays," *Carbon*, vol. 96, pp. 522–531, 2016.
- [40] L. Cheng, W. Guo, X. Cao, Y. Dou, L. Huang, Y. Song, J. Su, Z. Zeng, and R. Ye, "Laser-induced graphene for environmental applications: progress and opportunities," *Materials Chemistry Frontiers*, vol. 5, no. 13, pp. 4874–4891, 2021.
- [41] B. D. Abera, I. Ortiz-Gómez, B. Shkodra, F. J. Romero, G. Cantarella, L. Petti, A. Salinas-Castillo, P. Lugli, and A. Rivadeneyra, "Laser-induced graphene electrodes modified with a molecularly imprinted polymer for detection of tetracycline in milk and meat," *Sensors*, vol. 22, no. 1, p. 269, 2021.
- [42] L. X. Duy, Z. Peng, Y. Li, J. Zhang, Y. Ji, and J. M. Tour, "Laser-induced graphene fibers," *Carbon*, vol. 126, pp. 472–479, 2018.
- [43] M. Liu, J. Wu, and H. Cheng, "Effects of laser processing parameters on properties of laser-induced graphene by irradiating co₂ laser on polyimide," *Science China Technological Sciences*, vol. 65, no. 1, pp. 41–52, 2022.

- [44] Y. Chyan, R. Ye, Y. Li, S. P. Singh, C. J. Arnusch, and J. M. Tour, "Laser-induced graphene by multiple lasing: toward electronics on cloth, paper, and food," *ACS nano*, vol. 12, no. 3, pp. 2176–2183, 2018.
- [45] A. Behrent, C. Griesche, P. Sippel, and A. J. Baeumner, "Process-property correlations in laser-induced graphene electrodes for electrochemical sensing," *Microchimica Acta*, vol. 188, pp. 1–14, 2021.
- [46] R. Murray, M. Burke, D. Iacopino, and A. J. Quinn, "Design of experiments and optimization of laser-induced graphene," *ACS omega*, vol. 6, no. 26, pp. 16736–16743, 2021.
- [47] Y. Wang, G. Wang, M. He, F. Liu, M. Han, T. Tang, and S. Luo, "Multi-functional laser-induced graphene papers with combined defocusing and grafting processes for patternable and continuously tunable wettability from superlyophilicity to superlyophobicity," *Small*, vol. 17, no. 42, p. 2103322, 2021.
- [48] G. Reeves and H. Harrison, "Obtaining the specific contact resistance from transmission line model measurements," *IEEE Electron device letters*, vol. 3, no. 5, pp. 111–113, 1982.
- [49] S. Russo, M. Craciun, M. Yamamoto, A. Morpurgo, and S. Tarucha, "Contact resistance in graphene-based devices," *Physica E: Low-dimensional Systems and Nanostructures*, vol. 42, no. 4, pp. 677–679, 2010.
- [50] M.-C. Chen, C.-L. Hsu, and T.-J. Hsueh, "Fabrication of humidity sensor based on bilayer graphene," *IEEE Electron Device Letters*, vol. 35, no. 5, pp. 590–592, 2014.
- [51] J. Wu, Z. Wu, K. Tao, C. Liu, B.-R. Yang, X. Xie, and X. Lu, "Rapid-response, reversible and flexible humidity sensing platform using a hydrophobic and porous substrate," *Journal of Materials Chemistry B*, vol. 7, no. 12, pp. 2063–2073, 2019.
- [52] B. Kulyk, B. F. Silva, A. F. Carvalho, P. Barbosa, A. V. Girão, J. Deuermeier, A. J. Fernandes, F. M. Figueiredo, E. Fortunato, and F. M. Costa, "Laser-induced graphene from paper by ultraviolet irradiation: Humidity and temperature sensors," *Advanced Materials Technologies*, p. 2101311, 2022.
- [53] A. D. Smith, K. Elgammal, F. Niklaus, A. Delin, A. C. Fischer, S. Vaziri, F. Forsberg, M. Råsander, H. Hugosson, L. Bergqvist, *et al.*, "Resistive graphene humidity sensors with rapid and direct electrical readout," *Nanoscale*, vol. 7, no. 45, pp. 19 099–19 109, 2015.
- [54] H. Kun, L. Bin, M. Orban, Q. Donghai, and Y. Hongbo, "Accurate flexible temperature sensor based on laser-induced graphene material," *Shock and Vibration*, vol. 2021, pp. 1–7, 2021.